Journal of Integrative Neuroscience

J. Integr. Neurosci. **2025**; 24(12): 46163
https://doi.org/10.31083/JIN46163

Original Research

Spinal Dorsal Horn Neuronal Alterations Following CFA-Induced Inflammatory Pain in Mice

Hao Zheng[1], Xiaoyue Sun[1], Qingquan Yu[2], Xiaoyu Wang[1], Yangshuai Su[1], Xianghong Jing[1,*], Zhiyun Zhang[1,*]

[1]Institute of Acupuncture and Moxibustion, China Academy of Chinese Medical Sciences, 100700 Beijing, China
[2]Department of Scientific Research, The Affiliated Hospital of Jiangxi University of Chinese Medicine, 330006 Nanchang, Jiangxi, China
*Correspondence: jxhtjb@263.net (Xianghong Jing); zhangzhyun@yeah.net (Zhiyun Zhang)
Academic Editors: Vincent Lelievre and Bettina Platt
Submitted: 29 August 2025 Revised: 21 October 2025 Accepted: 21 November 2025 Published: 23 December 2025

Abstract

Background: The spinal dorsal horn (SDH) plays a crucial role in nociceptive processing. However, the temporal dynamics of neuronal excitability across different laminae during inflammatory pain remain incompletely understood. **Methods**: Complete Freund's adjuvant (CFA) was injected into the left hindpaw to induce inflammatory pain. Spontaneous pain behaviors were evaluated using CatWalk gait analysis and weight-bearing tests, while mechanical hypersensitivity was assessed using von Frey filaments. Neuronal activation patterns were mapped using c-Fos (a protein product of the *c-Fos* immediate-early gene) immunolabeling across superficial and deeper laminae of the SDH. Spontaneous and mechanically-evoked neuronal discharges were recorded *in vivo* using multi-electrode arrays. **Results**: Spontaneous pain behaviors were most pronounced during the first 3 days post CFA injection, with mechanical hypersensitivity persisting through day 7. A marked increase in c-Fos-positive neurons was observed specifically in superficial laminae on day 1, with no significant changes detected in the deeper laminae. Spontaneous and mechanically-evoked firing rates of SDH neurons increased significantly during days 1–5 post CFA injection. Importantly, wide dynamic range (WDR) neurons exhibited the greatest increase in evoked discharge frequency, while low-threshold mechanoreceptor (LTM) neurons showed the greatest proportional increase amongst neuronal subtypes. Furthermore, both WDR and LTM neurons shifted towards a more superficial distribution. **Conclusions**: Peripheral inflammatory pain induced distinct alterations in SDH neurons, characterized by an early increase in neuronal activities, followed by changes in the spatial distribution and proportion of WDR and LTM neurons.

Keywords: spinal cord dorsal horn; nociceptive pain; electrophysiological phenomena; multi-channel electrode

1. Introduction

The spinal dorsal horn (SDH) serves as the first relay station for somatosensory information in the central nervous system. It is organized into distinct laminae based on cellular architecture and function. The complex, interconnected network within this laminar organization plays a crucial role in modulating sensory inputs before they reach the supraspinal region [1]. Understanding alterations in neuronal excitability at a population level is critical for elucidating the spinal processing of nociception that underlies pathological pain conditions.

Neuronal populations in the SDH form synaptic connections with the central terminals of diverse primary sensory neurons in a spatially organized pattern [2]. Neurons in the superficial and intermedial SDH laminae predominantly receive nociceptive and innocuous information, respectively. Neurons in the deep laminae process both noxious and innocuous signals and are described functionally as having wide dynamic range (WDR). These multi-receptive neurons are predominantly distributed in the deep laminae (V–VI) [3], with sparse distribution in superficial laminae [4,5]. Nociceptive-specific (NS) neurons primarily synapse with Aδ and C afferents and respond to noxious inputs, while low-threshold mechanoreceptive (LTM) neurons selectively respond to innocuous stimuli. Historically, pain research has focused on examining the electrophysiological properties of WDR neurons under pathological pain conditions [6,7]. In comparison, the electrophysiological properties of the LTM and NS neurons are less comprehensively mapped [8]. However, the high neuronal heterogeneity and intricate microcircuit in the SDH suggest that the activity of a single group of neurons within one region may not accurately represent the overall dynamics of the larger network.

Electrophysiological techniques offer superior temporal resolution for monitoring neuronal activity while maintaining organism integrity. Previous single-unit *in vivo* recordings were often limited in their ability to achieve simultaneous population-level analysis. Although calcium imaging allows real-time, simultaneous assessment of activity across a vast majority of neurons in behaving animals, limitations persist in terms of recording depth and acquisition rate [9]. Multi-electrode arrays (MEAs) with integration of multiple microelectrodes enable simultaneous recording from multiple sites across different laminae of the dorsal horn. The application of this methodology in the rodent dorsal horn may lead to a better understanding of the

laminar differences within the SDH network [10]. MEA has been successfully employed in rat models to examine integrated signaling patterns among SDH neuronal populations [11,12]. Moreover, recent advances in MEA miniaturization have extended these recordings to both superficial and deep laminae in murine models.

In the present study, we systematically investigated functional changes in SDH neuronal excitabilities using complete Freund's adjuvant (CFA)-induced inflammatory pain mice. Nociceptive sensitization was evaluated through behavioral assessments of spontaneous pain and mechanical hyperalgesia, while SDH activation in laminae I–II was confirmed using c-Fos immunohistochemistry in combination with laminar-specific marker analysis. Finally, 32-channel MEA recording was employed to characterize population-level neuronal dynamics. This work revealed significant alterations in the firing rates, spatial distribution, and functional organization of distinct neuronal subpopulations within the SDH of mice with CFA-induced inflammatory pain.

2. Materials and Methods

2.1 Animals

A total of 95 healthy male C57BL/6J mice (age 6–8 weeks) without physical abnormalities and weighing 20–22 g [Beijing Vital River Laboratory Animal Technology Co., Beijing, China. license number: SCXK (Jing) 2021-006] were used in this study. The mice were allocated as follows: 49 for pain behavioral assays, 15 for immunofluorescence, and 31 for electrophysiological recordings. Cohorts did not overlap across assays. The animals were maintained under controlled environmental conditions with a 12-h light/dark cycle and a temperature of 24 $\pm$ 2 °C. Standard laboratory chow and water were provided *ad libitum*. All experimental procedures were approved by the Institutional Animal Care and Use Committee of the Institute of Acupuncture and Moxibustion, China Academy of Chinese Medical Sciences (approval no. D2024-01-26-09) and conducted in accordance with the National Institutes of Health Guide for the Care and Use of Laboratory Animals. After data collection, animals were euthanized with an overdose of inhaled isoflurane (R510-22-10, RWD Life Science Co., Shenzhen, Guangdong, China).

2.2 Establishment of the Inflammatory Pain Model and Group Assignment

For the CFA-treated group, mice received an intraplantar injection of 20 µL of CFA (F5881, Sigma-Aldrich, St. Louis, MO, USA) into the left hindpaw during isoflurane (R510-22-10, RWD Life Science Co.) inhalation anesthesia (1%–4%). The CFA solution was administered slowly and allowed to remain *in situ* for 2 minutes before withdrawal to ensure complete absorption, with no observable leakage detected. Mice that failed to develop CFA-induced paw inflammation (swelling/redness) were excluded (**Supplementary Fig. 1**). For the control group, naïve mice were used without sham handling or injection. For all experiments, mice were allocated to experimental groups using a computer-generated random number sequence upon completion of acclimatization. For behavioral cohorts, this randomization was performed after baseline behavior testing to ensure equivalent starting scores across groups.

2.3 Pain Behavioral Tests

Gait analysis was performed using the CatWalk XT system (version 10.6, Noldus Information Technology, Wageningen, The Netherlands) to observe spontaneous pain behaviors as previously described [13]. Briefly, the system consists of an enclosed walkway with a glass plate, illuminated by a fluorescent lamp that emits light inside the glass plate. Each mouse was placed individually in the CatWalk system and allowed to walk freely and traverse from one side of the walkway glass plate to the other. Where the mouse paws made contact with the glass plate, light was reflected down and the illuminated contact areas were recorded with a high-speed color video camera positioned underneath the glass plate. The recordings were carried out when the room was completely dark, except for light from the computer screen. The software automatically labeled all areas containing pixels above the set threshold and assigned them to the respective paws. Mice were trained to traverse the walkway for 2 days before baseline measurements. Animals were excluded if they failed to run voluntarily. Each mouse was tested at least three times. Five parameters were analyzed: (1) stand phase: duration in seconds of paw contact with the glass plate in a step cycle; (2) swing phase: duration in seconds of no paw contact with the glass plate in a step cycle; (3) duty cycle: stand duration as a percentage of the step cycle duration [stand / (stand + swing) $\times$ 100]; (4) single stance: duration in seconds of ground contact for a single paw; and (5) max contact max intensity: the maximum intensity of a paw at maximum paw-floor contact. These values were normalized by calculating the ratio between the ipsilateral (affected left hindpaw) and contralateral (unaffected right hindpaw) measurements to quantify the inflammatory response-induced alterations. Animals showing abnormal gait parameters before CFA injection were excluded (**Supplementary Fig. 1**).

To distinguish between inflammatory pain-induced gait alterations and potential motor deficits, motor coordination and balance were evaluated using the accelerating Rotarod test. Prior to testing, the mice underwent a 2-day habituation protocol on the Rotarod apparatus (Mouse-47650, Ugo Basile, Gemonio, Italy). The assessment was performed 24 h post CFA injection, with the Rotarod accelerating linearly from 0 to 40 rpm over a 300-s period. Three trials were conducted for each mouse, and both the latency to fall and terminal velocity were recorded.

In addition to gait analysis, spontaneous nociceptive behaviors were evaluated using a weight-bearing test system (model BIO-SWB-TOUCH-M, Bioseb, Vitrolles, France). Each mouse was placed in an acrylic glass chamber where independent force plates measured the weight distribution between hindpaws. After a 2-day habituation period, weight-bearing measurements were obtained by averaging the applied force (g) over a 10-s sampling period. The weight-bearing differential was calculated by subtracting the contralateral (right hindpaw) from the ipsilateral (CFA-injected left hindpaw) weight-bearing capacity. The final values represent the mean of six consecutive measurements. Animals showing imbalanced bilateral weight-bearing capacity before CFA injection were excluded (**Supplementary Fig. 1**).

Mechanical hypersensitivity was assessed using calibrated von Frey filaments (37450-275, Ugo Basile). Mice were individually housed in transparent glass chambers positioned on an elevated mesh platform. Prior to testing, animals underwent a habituation protocol consisting of 1-h sessions for 2 consecutive days, followed by a 30-min acclimation period before each test session. The mechanical withdrawal threshold was determined by applying von Frey filaments perpendicularly to the midplantar surface of the ipsilateral hindpaw with sufficient force to cause filament bending for 3–5 s. A response was considered positive if the animal exhibited any nocifensive behaviors, including brisk paw withdrawal, licking, or shaking of the paw, either during application of the stimulus or immediately after the filament was removed. Paw withdrawal thresholds were quantified using the modified Dixon up-down method [14,15]. The 50% threshold was calculated according to the formula: 50% threshold (g) = $10^{(X + kd)}/10^4$, where X represents the log unit value of the final filament, k is the tabular value for the pattern of positive/negative responses, and d denotes the mean difference in log units between filaments. Animals exhibiting abnormal mechanical sensitivity (withdrawal threshold <0.5 g or >1.5 g) under normal conditions were excluded (**Supplementary Fig. 1**).

Baseline measurements for gait parameters, weight-bearing distribution, and mechanical sensitivity were obtained 24 h prior to CFA (F5881, Sigma-Aldrich) injection, with subsequent assessments conducted on days 1, 3, 5 and 7 post injection. Motor coordination was evaluated using the Rotarod test. This was conducted only at the 24 h post-injection timepoint. All behavioral tests were performed at approximately 09:00 AM.

2.4 Immunofluorescence

Mice were deeply anesthetized with urethane (1.5 g/kg, U2500, Sigma-Aldrich) followed by transcardial perfusion with saline. It should be noted that no additional acute stimulation was conducted before perfusion. The lumbar spinal cord enlargements were harvested and fixed in 4% paraformaldehyde (PFA, P1110, Solarbio, Beijing, China), then dehydrated in 30% sucrose until the tissue sank to the bottom. After 24 h, the tissue was embedded in an optimal cutting temperature compound (4583, Sakura Finetek, Torrance, CA, USA), frozen, and sectioned at 30-µm thickness using a cryostat (CM1860, Leica, Wetzlar, Germany). The sections were collected in PBS-filled wells. Following PBS washing, the sections were blocked with 3% donkey serum (BMS0140, Abbkine, Wuhan, Hubei, China) and 0.5% Triton X-100 (T9284, Sigma-Aldrich) in PBS for 45 min at room temperature (RT). The sections were then incubated overnight at 4 °C in PBS containing 1% donkey serum and 0.5% Triton X-100, and the following primary antibodies: anti- isolectin B4 (IB4)-488 (1:500, I21411, Invitrogen, Carlsbad, CA, USA), mouse anti-protein kinase C-gamma (PKCγ) (1:300, 13-3800, Invitrogen), and rabbit anti-c-Fos (1:1000, ABE457, Millipore, Burlington, MA, USA). After three PBS washes, sections were incubated for 1.5 h at RT with secondary antibodies (donkey anti-mouse Alexa Fluor 647, 1:1000, ab150111, Abcam, Cambridge, UK; donkey anti-rabbit Alexa Fluor 555, 1:1000, ab150062, Abcam) and DAPI (1:50,000, D3571, Invitrogen) in PBS containing 1% donkey serum and 0.5% Triton X-100. Following the PBS washes, the sections were mounted on silane-coated slides and visualized using a confocal microscopy system (Nikon AX, Nikon Instruments Inc., Tokyo, Japan). An experienced researcher performed the quantification of c-Fos-positive cells, with the placement of the region of interest (ROI) borders illustrated in **Supplementary Fig. 2**.

2.5 Extracellular Recordings of SDH Neurons

In vivo extracellular recordings were performed from SDH neurons in L4–L6 segments. Mice were anesthetized with intraperitoneal urethane (1.5 g/kg, U2500, Sigma-Aldrich). A laminectomy was performed at T13 and L1 vertebrae to expose the lumbar enlargement (L4–L6). Following careful removal of the dura mater, the spine was immobilized using a stereotaxic frame (SR-6R-HT, Narishige, Tokyo, Japan) to minimize movement artifacts. The exposed spinal cord was continuously perfused with warm physiological saline. Core body temperature was maintained using a heating pad. Neural activity was recorded using a 32-channel silicon probe (A1×32-Poly2-5mm-50s-177, Neuronexus, Ann Arbor, MI, USA). This was inserted perpendicularly into the lateral hindpaw region of the dorsal horn at a depth of approximately 850 µm from the dorsal surface, and 300 µm lateral to the central vessel. The insertion procedure was carried out under a stereoscope (SZ61, Olympus, Tokyo, Japan) to confirm the spinal surface (defined as zero). A micromanipulator (DMA-1510, Narishige) was employed to guide insertion depth and lateral distance. The array was attached to the headstage. Signals were processed through a preamplifier (LB-0164-1, Blackrock Microsystems, Salt Lake City, UT, USA) with a bandpass filter of 250 Hz–5 kHz, digitized, and acquired using a neuronal signal acquisition system (Cerebus-128,

Cyberkinetics, Foxborough, MA, USA). Offline spike sorting and analysis were performed using Spike2 software (version 10.01a, Cambridge Electronic Design, Cambridge, UK). The quality control criteria for sorted units were as follows: (i) units were required to be well-isolated from noise and other units, quantified by an Isolation Distance >15 and an L-ratio <0.1; (ii) units had a refractory period violation rate of $\leq 2\%$; (iii) the signal-to-noise ratio (SNR) was required to be ≥ 3; (iv) units exhibited stable waveforms throughout the recording session, with no evidence of continuous monotonic drift; and (v) waveform shape was consistent across different stimulus conditions. Representative waveforms and autocorrelogram of a sorted single unit were shown in **Supplementary Fig. 3**.

The receptive fields (RFs) of recorded neurons were identified through mechanical probing of the ipsilateral hindpaw. Mechanical stimulation of the RFs consisted of brush stimulation using a camel-hair brush. Calibrated force was applied using an electronic rodent pincher (BIO-RPM, Bioseb) consisting of a pair of blunt forceps. One arm of the forceps was flat, while the opposing arm was tipped with a spherical cap 3.5 mm in diameter and 1 mm in height with smooth edges. For brush stimuli, the center of the hindpaw RF was stroked in the rostral to caudal direction about once per second for 15 s. For touch and pinch stimuli, the spherical cap was placed at the center of the hindpaw RFs. The applied force was then quickly increased by hand until it reached 40 g for touch stimulus and 150 g for pinch stimulus. This was held for 15 s using a timer. Stimuli were given in a predefined order (brush, 40 g touch, followed by 150 g pinch) in order to avoid potential diffuse noxious inhibitory controls (DNIC) elicited by the 150 g pinch. Each type of stimulus was given 2–3 times to improve reliability. The inter-trial interval was approximately 1–2 min to avoid neuronal fatigue in response to repeated stimuli. A 10-s stable response period (**Supplementary Fig. 4**) from each 15-s mechanical stimulus was analyzed to minimize artifacts from potential hand movements. The spontaneous firing rates were defined as the mean frequency of a 30-s baseline period before any stimulation. The stimulus-evoked firing rates were defined as the mean frequency of the 10-s stable response window minus the mean frequency of the 10-s pre-stimulus baseline. Recordings containing fewer than three neurons per animal were excluded to ensure an adequate sample size for population-level analysis (**Supplementary Fig. 1**).

Neurons were classified into three distinct categories based on their response properties to mechanical stimulation as described previously [16]: (1) LTM neurons that responded exclusively to innocuous stimuli (dynamic brush and/or static touch); (2) WDR neurons that exhibited graded responses to both innocuous and noxious stimuli (pinch), with greater responses to the latter; and (3) NS neurons that responded selectively to noxious pinch.

The depth of each probe was calculated based on the distance from the electrode tip to the spinal cord surface and the spacing between probes. The depth bin for analysis was set as 25 µm. It should be noted that tissue edema caused by surgery and exposure of the spinal cord beyond control may alter the estimated depths. Other potential limitations such as the tilt of the electrode tip and zeroing deviation were controlled as described in the insertion procedure above.

2.6 Statistical Analysis

All data are presented as the mean ± SEM. Statistical analyses were performed using GraphPad Prism (version 9.0, GraphPad Software Inc., San Diego, CA, USA) and SPSS (version 26.0, IBM Corp., Armonk, NY, USA). The Shapiro-Wilk test was used to assess the normality of data distribution (SPSS 26.0). For normally distributed data, comparisons between two groups were made using the unpaired Student's *t*-test (SPSS 26.0). Time course comparisons between groups were analyzed using two-way ANOVA followed by Šídák's multiple comparisons test (GraphPad Prism 9.0). For non-normally distributed data, comparisons between multiple groups were performed using the Kruskal-Wallis test, followed by Dunn's multiple comparisons test (GraphPad Prism 9.0). Differences were considered statistically significant at $p < 0.05$, $p < 0.01$, and $p < 0.001$. A list of key resources used in this study was shown in **Supplementary Table 1**.

3. Results

3.1 Pain-Related Behaviors in Mice With CFA-Induced Inflammatory Pain

CatWalk gait analysis was performed to objectively evaluate pain-induced locomotor alterations. This method has been used previously to assess mechanical allodynia in animal models [17]. As shown by the timing view and footprint intensities (Fig. 1A), CFA-treated mice exhibited significant alterations in their bilateral hindlimb stepping pattern. Compared with baseline measurements, CFA-treated mice showed notable reductions in stand phase duration (Fig. 1B), duty cycle (Fig. 1D), single stance duration (Fig. 1E), and max contact max intensity (Fig. 1F) of the affected hindpaw, together with an increase in the swing phase duration (Fig. 1C). These abnormalities were most prominent during the first 3 days post CFA injection, suggesting peak spontaneous pain during this period. However, gait parameters showed a gradual recovery beginning on day 5. To exclude potential motor dysfunction induced by CFA injection, we also performed Rotarod testing. Both the latency and maximal rotational velocity at fall remained unchanged in CFA-treated mice compared with controls (Fig. 1G), indicating the observed gait abnormalities were primarily pain-driven rather than because of motor impairment. We also examined complementary weight-bearing balance and reflexive pain-related behaviors. Both these measurements revealed that CFA-treated

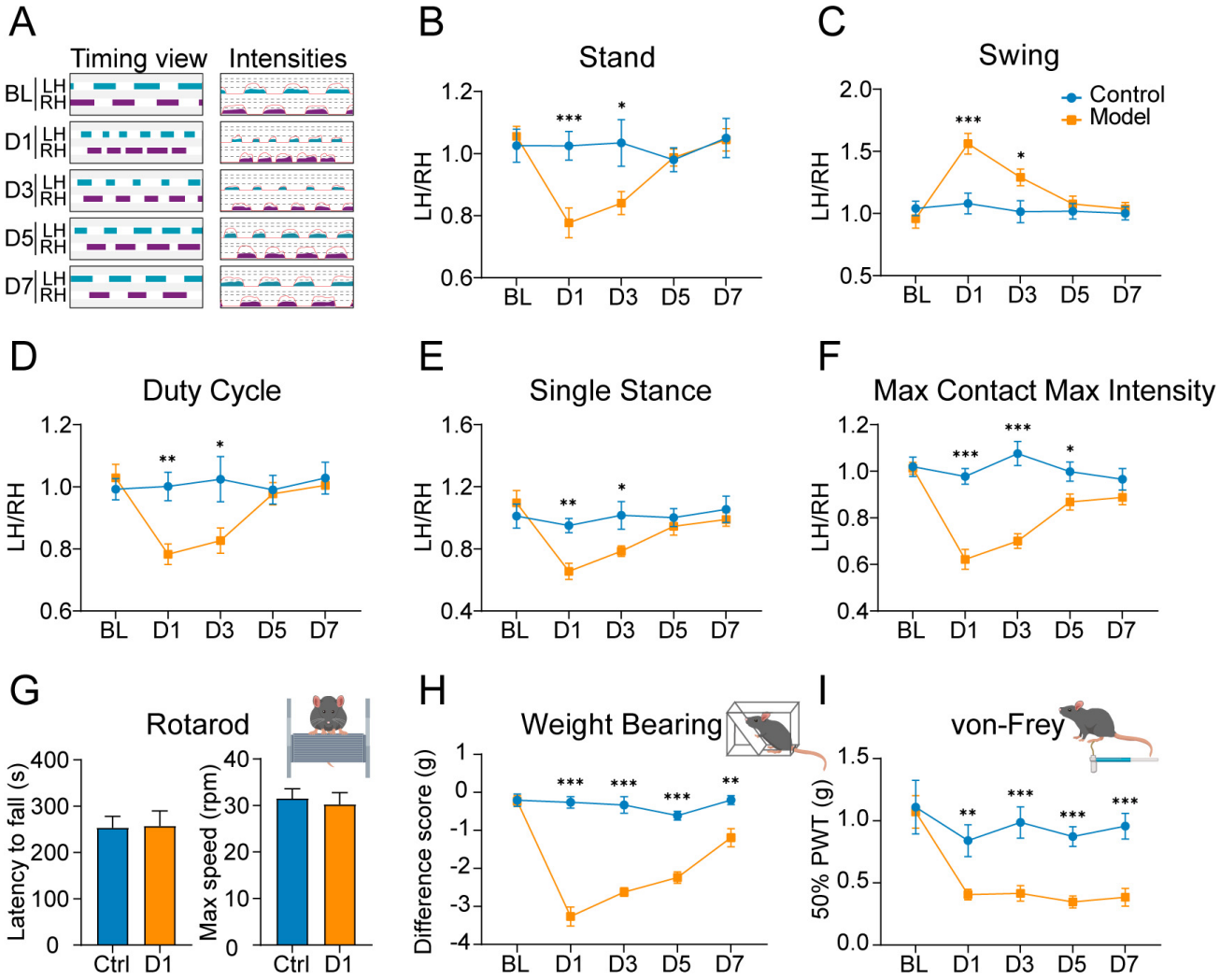

Fig. 1. CFA-induced inflammatory pain induces time-dependent changes in spontaneous and evoked pain behaviors. (A) Representative CatWalk gait analysis showing timing views (left) and pressure intensity maps (right) of hindpaw prints in control mice and at the indicated time points after CFA injection (days 1, 3, 5 and 7). (B–F) Quantitative analysis of various gait parameters assessed by CatWalk: (B) stand phase duration, (C) swing phase duration, (D) duty cycle, (E) single stance duration, and (F) max contact max intensity. Data were collected from control mice and CFA-treated mice. Values were normalized as the ipsilateral (affected left hindpaw)/contralateral (unaffected right hindpaw) ratio. Mean ± SEM (control, n = 8, CFA-treated, n = 9; * $p < 0.05$, ** $p < 0.01$, *** $p < 0.001$ vs. control; two-way ANOVA with Šídák's test). (G) Motor coordination was assessed by the Rotarod test on day 1 post-CFA injection. Left: latency to fall (seconds); Right: maximal rotational velocity at fall (rpm). Mean ± SEM (control, n = 8, CFA-treated, n = 9; unpaired Student's *t*-test). (H) Weight bearing measured as the difference between ipsilateral and contralateral hindpaws (grams) after CFA injection. Mean ± SEM (Control, n = 8; CFA-treated, n = 8; ** $p < 0.01$, *** $p < 0.001$ vs. control; two-way ANOVA with Šídák's test). (I) Mechanical hypersensitivity measured by the von Frey filament test and showing paw withdrawal thresholds for the ipsilateral hindpaw. Mean ± SEM (control, n = 8, CFA-treated, n = 8; ** $p < 0.01$, *** $p < 0.001$ vs. control; two-way ANOVA with Šídák's test). Adobe Illustrator 2020 (version 24.1.3, Adobe Inc., San Jose, CA, USA) was used to create the illustrations in (G–I). CFA, complete Freund's adjuvant; SEM, standard error of the mean; ANOVA, analysis of variance; BL, baseline; LH, left hindpaw; RH, right hindpaw.

mice exhibited sustained spontaneous pain and evoked hypersensitivity, especially in von Frey filament-evoked mechanical allodynia (Fig. 1H,I). While gait analysis indicated partial recovery by at least day 5, weight-bearing asymmetry and decreased mechanical withdrawal thresholds persisted through day 7. Collectively, these behavioral analyses demonstrate that intraplantar CFA injection induces both dynamic temporal changes and persistent static pain.

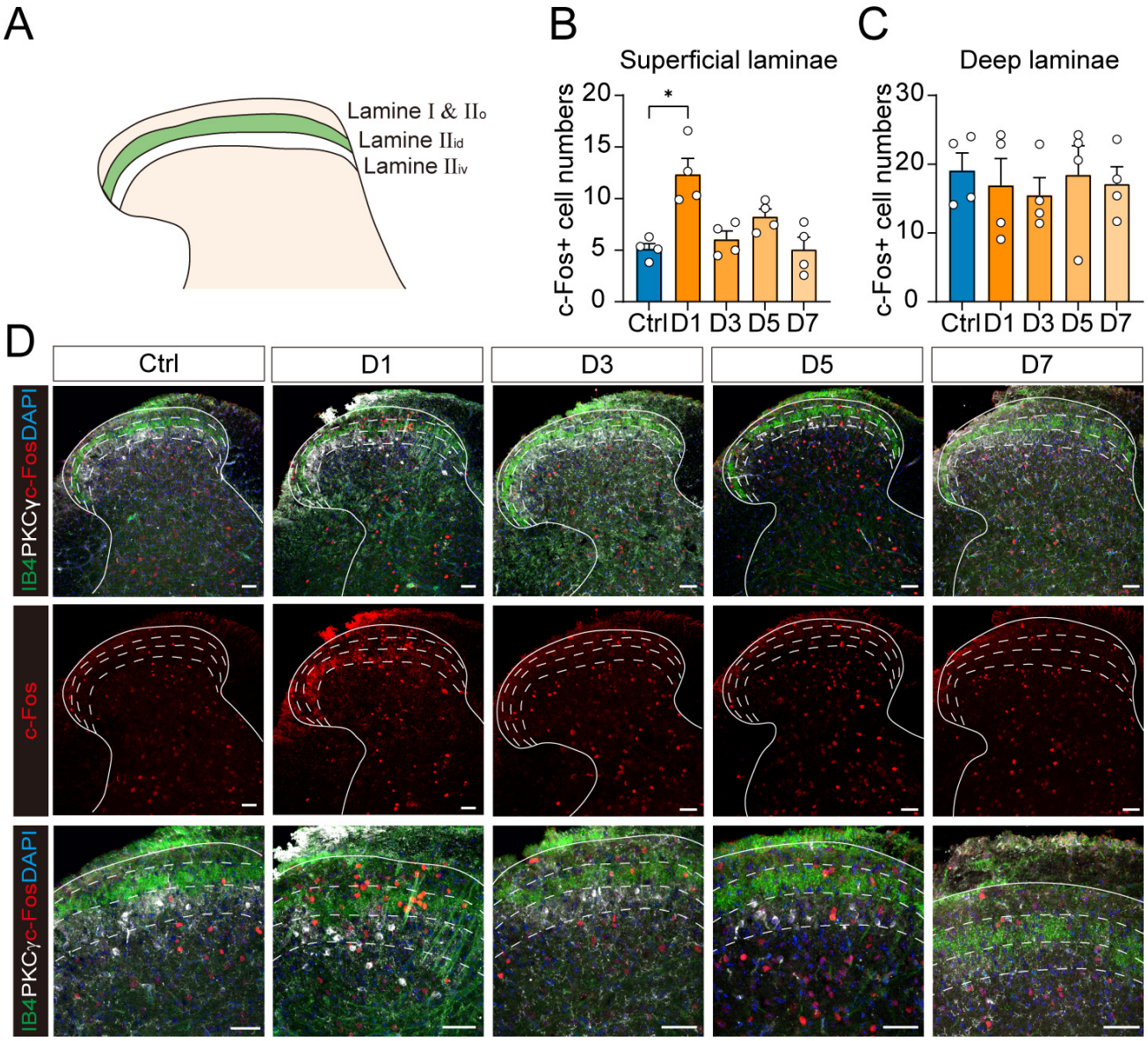

Fig. 2. Time-dependent c-Fos expression across superficial and deep laminae of the SDH after CFA injection. (A) Schematic representation of mouse spinal dorsal horn showing lamina II_i delineated by IB4 (green) and PKCγ (white) immunostaining. (B,C) Quantitative analysis of c-Fos positive neurons in superficial (lamina I–II, B) and deep laminae (lamina III–V, C) of the dorsal horn at indicated time points after CFA injection. (n = 4 mice per group). Mean ± SEM (* $p < 0.05$ vs. control; Kruskal-Wallis test with Dunn's test). Effect sizes and 95% confidence intervals of the data was shown in **Supplementary Table 2**. (D) Representative immunofluorescence images showing c-Fos expression (red) in superficial (lamina I–II) and deep laminae of the dorsal horn in control and CFA-treated mice across different time points (days 1, 3, 5, and 7). Scale bars: 50 µm. Adobe Illustrator 2020 (version 24.1.3, Adobe Inc.) was used to create the illustrations in (A). SDH, spinal norsal horn; IB4, isolectin B4; PKCγ, protein kinase C-gamma.

3.2 Laminar-Specific Distribution of c-Fos in the SDH Following CFA-Induced Inflammatory Pain

Protein expression of the immediate early gene *c-Fos* has been widely used as a marker for neuronal activation [18]. To study dynamic and laminar-specific sensory processing in the SDH, we examined the temporal and spatial distribution of c-Fos expression across distinct SDH laminae following CFA injection. IB4 and PKCγ were employed as laminar-specific markers to delineate the inner dorsal (II_{id}) and ventral (II_{iv}) boundaries of lamina II, respectively [19] (Fig. 2A). SDH regions were categorized accordingly into superficial (laminae I–II) and deep (laminae III–V) domains. Quantitative analysis revealed minimal c-Fos expression in the superficial laminae of control mice. As expected, CFA induced a significant increase in c-Fos positive neurons within the superficial laminae on day 1, when the mice displayed obvious nociceptive behaviors (Fig. 2B,D). However, the elevated c-Fos expres-

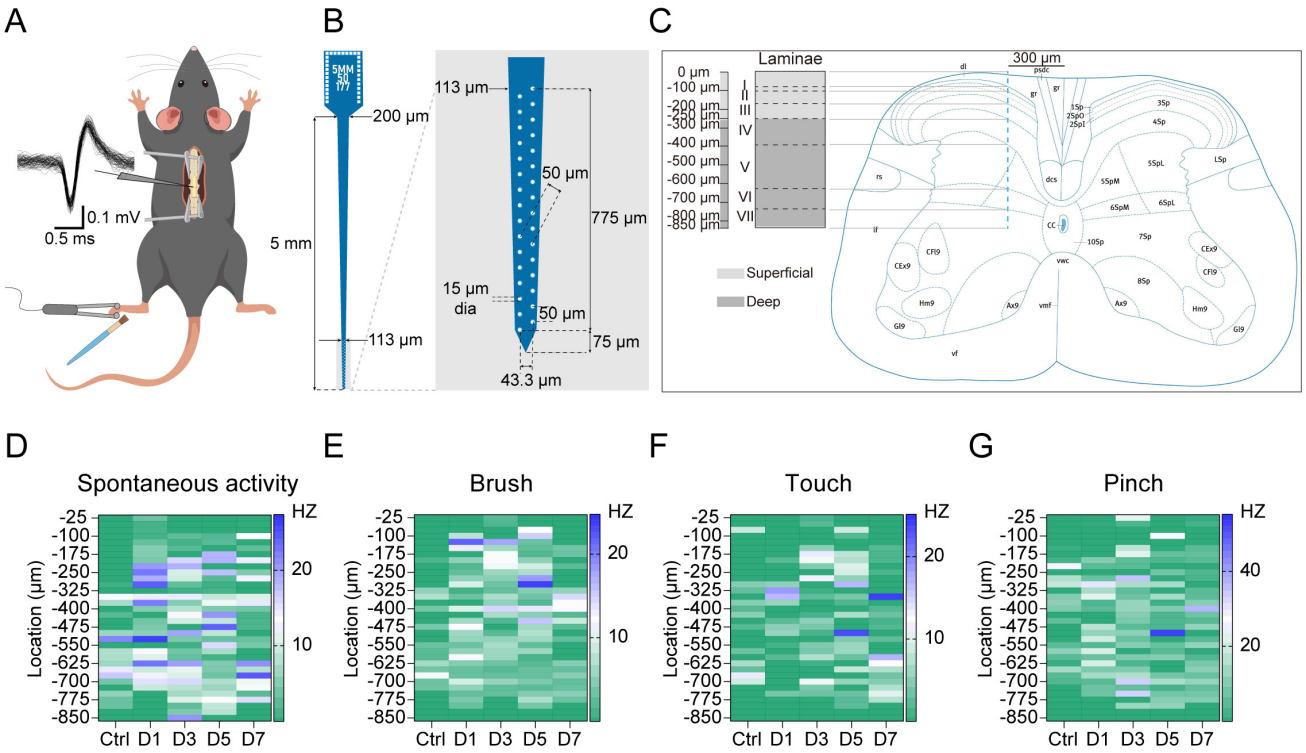

Fig. 3. Temporal changes in spontaneous and evoked neuronal activity across different depths of the SDH after CFA injection. (A) Experimental setup for *in vivo* SDH neuronal recordings. A 32-channel MEA was used to record action potentials from SDH neurons while applying mechanical stimuli (touch, brush and pinch) to the ipsilateral hindpaw receptive fields. (B) Configuration of the 32-channel microelectrode array showing the recording sites distributed across an 850 µm depth. (C) Predicted extent and borders of spinal laminae across the 850 µm depth for 300 µm lateral to the middle spinal artery. The SDH laminar organization were divided into superficial (0–250 µm) and deep (250–850 µm) regions. The annotated L4 spinal cord section was adapted from the Mouse Spinal Cord Atlas provided by the Allen Institute for Brain Science (https://mouse.brain-map.org/experiment/siv?id=100050402&imageId=101006501&imageType=atlas). (D–G) Depth-dependent neuronal activity represented as heatmaps and showing (D) spontaneous, (E) brush-evoked, (F) touch-evoked, and (G) pinch-evoked firing rate changes (Hz). Depth bin for each row was 25 µm. The color scale represents the firing frequency in Hz. Animal numbers: control: n = 6; day 1: n = 6; day 3: n = 6; day 5: n = 7; day 7: n = 6. Temporal profile of spontaneous and evoked neuronal activity in the superficial and deep dorsal horn following CFA injection. A detailed analysis of spontaneous and evoked neuronal activity across the superficial and deep SDH is presented in **Supplementary Fig. 5** and **Supplementary Table 3**. Adobe Illustrator 2020 (version 24.1.3, Adobe Inc.) was used to create the illustrations in (A–C). MEA, microelectrode array.

sion decreased to normal levels after day 3. In addition, the number of c-Fos positive neurons in the deep laminae remained comparable with control levels (Fig. 2C,D). These results suggest that enhanced neuronal activation in superficial SDH laminae may represent a key neural substrate underlying the manifestation of spontaneous pain in CFA-induced inflammation.

3.3 Spontaneous and Evoked Mechanical-Excitability of SDH Neurons

A comprehensive view of real-time neuronal responsiveness in persistent inflammatory pain was obtained using multi-lamina extracellular recordings to characterize the spatiotemporal dynamics of neuronal excitability throughout the dorsal horn. Conventional c-Fos mapping fails to detect this. Neurons in the SDH were categorized into superficial (0–250 µm) and deep regions (250–850 µm) based on the locations of their recording (Fig. 3A–C, Ref. [20] for C). Each experiment yielded an average of 12 isolated single units per mouse.

Heatmap analysis showed laminar-specific differences in spontaneous and evoked neuronal activity between control and CFA-treated mice. In control animals, neurons in the superficial laminae exhibited minimal activity, whereas deep laminae displayed higher levels of spontaneous firing (Fig. 3D). Following CFA injection, the spontaneous excitabilities of neurons among all laminae increased rapidly on day 1, then gradually declined to normal levels (Fig. 3D). As for evoked activity, neurons across all laminae displayed limited responses to mechanical stimuli under physiological conditions. In mice injected with CFA, brush stimulus elicited the most pronounced neuronal activity in the superficial laminae, whereas touch and pinch

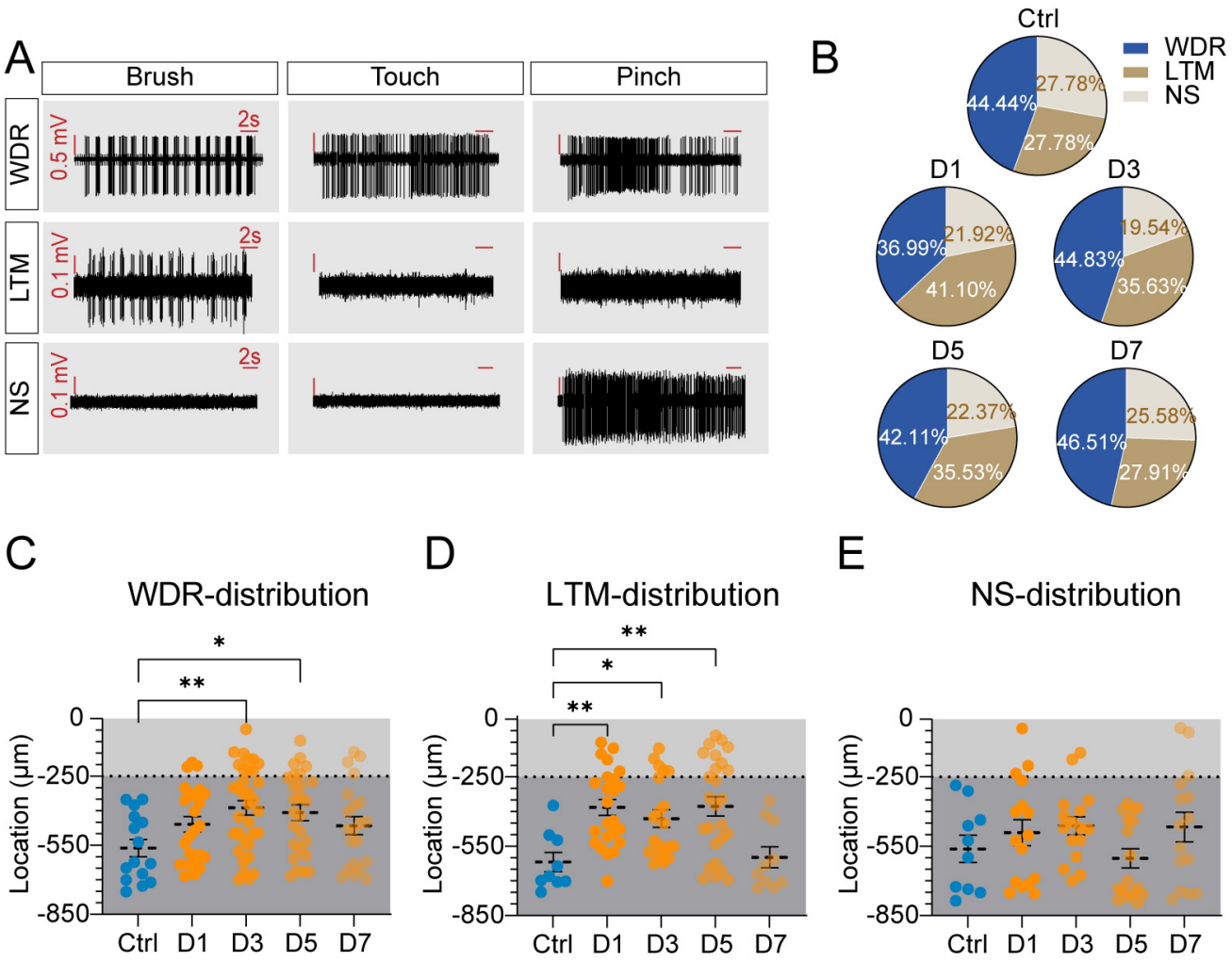

Fig. 4. Temporal changes in neuronal subtypes and their spatial distribution in SDH following CFA-induced inflammatory pain. (A) Representative response patterns defining neuronal subtypes. WDR neurons show graded responses to brush, touch, and pinch stimuli. LTM neurons respond only to brush stimulation, while NS neurons respond exclusively to pinch stimulation. (B) Proportion of neuronal subtypes (WDR, LTM, and NS) in control mice and inflammatory pain mice at indicated time points. Values are shown as the percentages of total recorded neurons. (C–E) Spatial distribution analysis of recorded neurons across dorsal horn depth: (C) WDR neurons (control, N = 16; day 1, N = 27; day 3, N = 40; day 5, N = 32; day 7, N = 27). (D) LTM neurons (control, N = 10; day 1, N = 30; day 3, N = 28; day 5, N = 27; day 7, N = 12). (E) NS neurons (control, N = 10; day 1, N = 16; day 3, N = 17; day 5, N = 17; day 7, N = 16). N represents neuron number (animal n values match Fig. 3). Scatter plots display the depth distribution, where light, and dark gray regions correspond to superficial and deep laminae, respectively. Values are presented as the mean ± SEM. Statistical significance was determined using Kruskal-Wallis test followed by Dunn's multiple comparisons. * $p < 0.05$, ** $p < 0.01$ vs. control. WDR, wide dynamic range; LTM, low-threshold mechanoreceptive; NS, Nociceptive-specific.

stimuli induced comparable neuronal hyperactivity across all laminae (Fig. 3E–G).

Collectively, these electrophysiological recordings suggest that neurons across the dorsal horn in mice with inflammatory pain tend to exhibit an increase in spontaneous and evoked excitability. The temporal profile of these alterations correlates well with both spontaneous and evoked pain behaviors, providing a more comprehensive understanding of the neuronal basis of inflammatory pain processing.

3.4 Alterations in Mechanically-Responsive Neuronal Populations in the SDH During Inflammatory Pain

To further elucidate the neuronal population underlying inflammatory pain, the proportion and distribution of SDH neurons were characterized across three functional subtypes: WDR, LTM, and NS neurons. Mechanical response was assessed using dynamic brush and static touch as innocuous stimulation, and a 150-g calibrated forceps pinch was used as noxious stimulation. Neurons responding to both stimuli were classified as WDR, while neurons

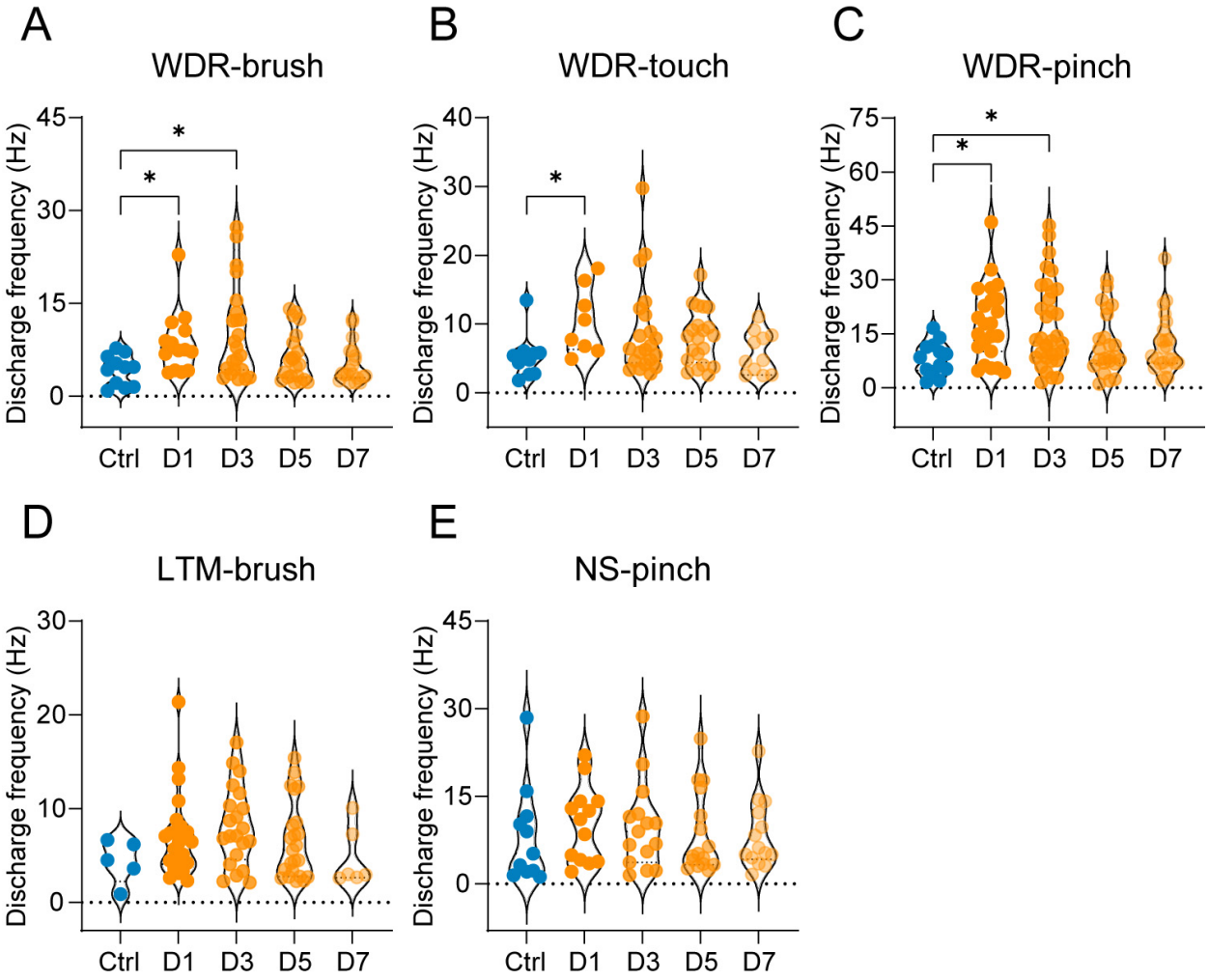

Fig. 5. Temporal changes in stimulus-evoked responses of distinct neuronal subtypes after CFA injection. (A–C) Analysis of WDR neuron firing rates in response to (A) brush, (B) touch, and (C) pinch stimulation. (D) Brush-evoked firing rates of LTM neurons. (E) Pinch-evoked firing rates of NS neurons. Values are presented as individual data points on violin plots (N values for neurons as shown in Fig. 4). Statistical significance was determined using Kruskal-Wallis test followed by Dunn's multiple comparisons. * $p < 0.05$ vs. control. See **Supplementary Fig. 6** for a detailed analysis of WDR neuron responses to mechanical stimuli across days.

responding exclusively to innocuous stimuli were LTM, and neurons responding exclusively to noxious stimuli were NS (Fig. 4A). Quantitative analysis revealed dynamic shifts in the composition of mechanically-responsive neuronal populations (Fig. 4B). Under physiological conditions, WDR neurons constituted the predominant population (44.44%) of recorded neurons, whereas LTM and NS neurons were present in comparable proportions (27.78%). On day 1 after CFA injection, the proportion of WDR neurons decreased markedly (36.99%) but returned to prominence in later observations. LTM and NS neurons exhibited divergent dynamics at day 1, with LTM peaking at 41.10%, whereas NS neurons declined to 21.92%. Both neuronal subtypes gradually returned to baseline levels thereafter.

Spatial distribution analysis revealed a shift in depth of the neuronal populations following inflammatory pain. WDR neurons, which normally predominate in deeper laminae, exhibited a significant shift toward more superficial locations on days 3 and 5 (Fig. 4C, **Supplementary Table 4**). LTM neurons were typically concentrated in deep laminae under normal conditions, but showed an enhanced superficial distribution on days 1, 3, and 5 post-CFA compared with controls (Fig. 4D, **Supplementary Table 4**). The distribution of NS neurons remained unchanged throughout the observation period (Fig. 4E, **Supplementary Table 4**). The concurrent superficial shift of both LTM and WDR neurons suggests enhanced nociceptive processing through increased integration of both noxious and innocuous inputs in pain-processing circuits. Overall, alterations in both the proportion and distribution of SDH neurons may represent a form of maladaptive plasticity that contributes to the heightened pain sensitivity observed in our behavioral studies.

3.5 Subtype-Specific Changes in the Mechanical Sensitivity of SDH Neurons Following CFA-Induced Inflammatory Pain

After characterizing the changes in proportion and distribution of SDH neurons, we next assessed their mechanical excitabilities by quantifying evoked discharges in response to various stimuli (brush, touch, and pinch) following CFA injection. The discharge frequency of WDR neurons evoked by brush and pinch stimuli was significantly higher on days 1 and 3 post CFA injection compared with controls. Additionally, these neurons showed increased mean firing frequency to touch specifically on day 1 (Fig. 5A–C). Interestingly, despite their altered proportion and distribution patterns, LTM neurons in mice with inflammatory pain showed a slight increase in their brush-evoked excitabilities (Fig. 5D). NS neurons maintained relatively stable activities to pinch stimuli throughout the observation period (Fig. 5E). The differential evoked activities of WDR, LTM, and NS neurons suggests that WDR neurons serve as key cellular mediators for the manifestation of both mechanical allodynia and hyperalgesia in inflammation.

4. Discussion

In the present study we utilized immunofluorescence and extracellular recordings to systematically investigate changes in SDH neuronal excitability that underlie nociceptive behaviors in inflammatory pain. Our results demonstrate that spontaneous nociceptive behaviors in mice with CFA-induced inflammatory pain exhibit parallel temporal dynamics with SDH neuronal hyperactivity. Furthermore, pathological pain states induced significant shifts in the depth, proportion and stimulus-responsive profiles of SDH neuronal subpopulations. Moreover, WDR hypersensitivity and an increased proportion of LTM neurons were the most robust electrophysiological correlates of inflammatory pain development.

Objective assessment of nociceptive somatosensory responses in animal models requires reliable behavioral assays [21]. Von Frey testing is an established, standardized metric for evoked nociception in pain research, based on the consistently decreased withdrawal thresholds observed in rodents. Pain-affected animals frequently exhibit spontaneous behaviors including tactile hypersensitivity in the injured region and compensatory postural adjustments. The present study incorporated gait analysis and weight-bearing tests to evaluate spontaneous pain, alongside von Frey testing for mechanical sensitivity assessment. Consistent with a previous study [22], our results demonstrated transient gait alterations accompanied by progressive restoration of bilateral weight-bearing balance in mice with inflammatory pain, together with persistent hyper-responsiveness to mechanical stimuli. Unlike murine models of neuropathic and osteoarthritic pain which exhibit persistent gait abnormalities for several weeks [23,24], our inflammatory pain model showed complete resolution within 5 days post CFA injection. This divergence may originate from the self-limiting nature of inflammatory processes, which differs fundamentally from the chronic and maladaptive neuroplasticity observed in neuropathic and osteoarthritic conditions. Therefore, timepoints and a diversity of behavior assessments are of great importance for the study of pain conditions in animals.

The SDH functions as the primary central sensory integration site, with discrete laminae exhibiting specialized functional segregation [25]. Nociceptive Aδ- and C-fibers predominantly synapse within superficial laminae, while myelinated low-threshold mechanoreceptive afferents terminate at deeper laminae [1]. Laminae I–II contain nociceptive projection neurons that directly transmit signals to supraspinal centers, whereas deeper laminae (III–IV) primarily consist of heterogeneous excitatory and inhibitory interneurons that form modulatory microcircuits [26]. To assess alterations in SDH neuronal activity at specific time points within a 7-day period, we examined the expression of immediate early genes together with lamina-specific markers. Since its initial characterization in the spinal cord following noxious stimulation [18], c-Fos has been widely validated and is an established marker for identifying nociception-related neuronal activity in somatosensory studies [27,28]. FosB and its splice variant Delta FosB (ΔFosB) also serve as important markers of cellular activation. Because of its extended half-life and cumulative expression upon repeated or chronic stimulation, ΔFosB is an excellent marker of long-term neuronal adaptations and has been widely utilized in studies of chronic neurological conditions [29,30]. However, the persistent nature of ΔFosB makes it less suitable for resolving discrete, time-limited activation events. While capable of reflecting acute responses, FosB has been primarily characterized in non-neuronal tissues, such as epithelial cells, vascular endothelial, and immune cells [31,32]. Importantly, both FosB and ΔFosB are largely confined to the brain, with limited characterization in the SDH. Therefore, given its well-documented expression profile and strong association with nociceptive processing in the dorsal horn, c-Fos represents an appropriate choice for detecting subacute neuronal responses within the present experimental timeframe. Under physiological conditions, neurons in superficial laminae are under tonic inhibition and show minor activation [33], as revealed in our c-Fos labelling experiment. However, these neurons can be selectively activated by noxious thermal or mechanical stimuli [28,34]. Consistent with a previous study [35], mice with inflammatory pain showed a marked increase in c-Fos$^+$ neurons in superficial but not deeper laminae on day 1 post CFA injection, correlating temporally with peak spontaneous pain behaviors. The observed expression of c-Fos in SDH neurons, while significant in our inflammatory pain context, was comparatively lower than in a previous neuropathic pain study [36]. This is likely because neuropathic pain involves more severe

and sustained central sensitization [37], whereas the Fos-labeled neuronal activation in our study primarily reflects ongoing spontaneous activity in the absence of any exogenous mechanical stimulation. This pattern demonstrates a massive noxious ascending projection that underlies the potential mechanisms of spontaneous pain.

It should be noted that the subsequent reduction in superficial c-Fos$^+$ neurons does not preclude the persistence of nociception. Our electrophysiological recordings showed lasting hyperexcitability in both spontaneous and evoked neuronal responses across SDH laminae, indicating a spatial expansion of sensitization during chronic pain maintenance. Interestingly, we observed that dynamic brush stimulus induced a higher neuronal discharge frequency than static touch. This parallels the well-established behavioral dissociation between dynamic allodynia and static hyperalgesia in both clinical and preclinical pain models [38–40]. Genetic manipulation studies further demonstrate that distinct neural circuits mediate these differential sensory phenotypes [41,42]. Our findings extend this dichotomy to the level of spinal neuronal response, suggesting that laminar-specific plasticity underlies modality-selective pain hypersensitivity.

In vivo electrophysiological recordings have primarily been performed in rats because of their technical accessibility [43,44]. However, in a recent study we successfully implemented this methodology in murine SDH using MEA. Building upon a prior innovative framework [6,45,46], our high-density 32-channel MEA with 50-µm inter-electrode spacing enabled depth-resolved monitoring of neuronal population dynamics during CFA-induced inflammatory pain progression. Neurons were categorized into LTM, WDR, and NS, based on stimulus-response profiles, as previously described [47,48]. Interestingly, all three neuronal populations exhibited significant plasticity, as evidenced by both their shifts in proportion and laminar distribution patterns. Peripheral inflammation in mice induced a particularly pronounced increase in the proportion of LTM neurons, along with a ventral-to-dorsal shift of all three neuronal types. This spatial reorganization aligns with previous reports of altered neuronal distribution in the SDH under pathological pain conditions [49]. The observed alteration may partly be attributed to impaired inhibitory transmission. Under physiological conditions, GABAergic and glycinergic neurons inhibit the activation of neurons in superficial laminae by large-diameter, non-nociceptive afferents [50,51]. In inflammatory states, however, these inhibitory circuits become modified and lead to enhanced responses in superficial laminae to low-threshold peripheral inputs [52–54]. Such disinhibition represents a key mechanism underlying touch-evoked pain-like behaviors [35,55,56], consistent with the persistent mechanical allodynia observed in our von Frey tests.

While WDR neurons are considered predominantly located in the deep dorsal horn, numerous studies have confirmed their presence in laminae I and II [4,57,58]. Our data similarly demonstrated an appearance of WDR neurons in superficial laminae in inflammatory pain mice. Besides, a previous study of cancer pain models has reported a shift from NS to WDR predominance in superficial layers [59]. However, this specific transition was not observed in our inflammatory pain model. This discrepancy may stem from the less severe and distinct pathophysiology of inflammatory pain compared with neuropathic or cancer-related pain states. Furthermore, our electrophysiological recordings captured a greater number of active neurons in mice with inflammatory pain than in those under normal conditions. This likely results from inflammatory mediators sensitizing previously unresponsive sensory afferents and enhancing presynaptic glutamate signaling [60,61]. The resultant increase in excitatory drive may recruit once-silent dorsal horn neurons, explaining the increased number of recorded units [62]. Therefore, the observed shifts in neuronal subtype proportions not only derive from neuronal functional modification in the dorsal horn, but also likely attribute to functional recruitment of previously silent neurons into the active network.

Spinal WDR neurons encode mechanical stimulus intensity through changes in firing rate, which not only increase with escalating stimulus intensity but also exhibit hyperactivity under various pathological pain conditions [43,63]. Accordingly, the discharge frequency of WDR neurons serves as a valuable indicator for assessing nociceptive transmission in the SDH. These neurons integrate inputs from large-diameter primary afferents, Aδ-nociceptors, as well as polysynaptic C-fibers [48]. Therefore, their firing patterns reflect convergent signaling from multiple primary afferent types. Importantly, WDR neuronal discharge evoked by suprathreshold electrical stimulation can be separated into early component mediated by Aβ-fibers, and later component mediated by Aδ- and C-fibers [64]. Based on latency, multiple studies have shown that the hyperexcitability of WDR neurons in pathological pain states is primarily driven by enhanced input from Aδ- and C-fibers, rather than Aβ-fibers [65,66]. In the present study, noxious pinch stimuli evoked more robust WDR discharges than innocuous brush or touch. Furthermore, WDR neurons in mice with inflammatory pain exhibited significantly increased responsiveness to peripheral stimulation. However, the temporal resolution of our mechanical stimulation precludes a definitive assignment of this hyperresponsiveness to Aβ-, Aδ-, or C-fiber-mediated pathways.

Additionally, a previous study indicates that WDR neurons exhibit greater sensitivity to peripheral stimulation than LTM and NS neurons [67]. Our data similarly demonstrated that WDR neurons displayed heightened activity that coincided with spontaneous pain behaviors on the 1st and 3rd days after CFA injection, as evidenced by gait abnormalities. Notably, neither LTM nor NS subtypes showed similarly pronounced changes in evoked discharge

frequency. This differential response may be attributed to injury-related sensitization specific to WDR neurons, a phenomenon not observed in NS subtypes [68]. However, this correlation between neuronal activity and pain behaviors derives from separate cohorts for terminal electrophysiology and behavioral testing. Future studies employing chronic recording techniques would be valuable to establish definitive causal links between individual neuronal response profiles and the manifestation of specific pain behaviors. Besides, methodological considerations regarding neuronal receptive fields should be noted. To ensure consistent laminar localization, the lateral recording position was fixed across experiments. Meanwhile, unlike single-unit recordings that identify receptive fields based on individual neuronal responses, our approach defined receptive fields as locations eliciting multi-unit activity. Given that WDR neurons possess broad receptive fields that expand further under pathological conditions [47], our recordings likely overrepresented WDR neuronal responses. This sampling bias should be considered when interpreting the observed discharge patterns.

There are several limitations to our study. First, while anesthesia allows stable acute recordings, it unavoidably masks the dynamics of chronic pain. Emerging technologies such as ultra-flexible electrode arrays enable longitudinal spinal monitoring in awake mice [69], although further validation of their signal stability and efficacy is needed. These advanced tools may provide new opportunities to investigate spinal sensory processing under natural pain conditions. Additionally, our classification of SDH neurons relied exclusively on mechano-sensitivity without specific neurochemical markers, reflecting a fundamental constraint of current *in vivo* electrophysiological approaches. Future research should focus on developing multimodal methodologies that combine morphological characterization with *in vivo* electrophysiology, thereby enabling more comprehensive functional analysis of neuronal populations.

5. Conclusions

The spontaneous pain behaviors observed in mice with inflammatory pain exhibited parallel dynamics with SDH neuronal hyperactivity. Following CFA-induced inflammation, SDH neuronal subpopulations underwent significant shifts in depth and proportion, and exhibited altered stimulus-responsive profiles. Among these alterations, the sensitization of WDR neurons and expansion of the LTM population served as dominant mechanisms of inflammatory pain pathogenesis.

Availability of Data and Materials

The data that support the findings of this study are available from the corresponding author upon reasonable request.

Author Contributions

HZ: Investigation, Methodology, Formal analysis, Writing original draft. XS: Investigation, Methodology, Writing review & editing. QY: Investigation, Methodology, Writing review & editing. XW: Methodology, Resources, Validation, Writing review & editing. YS: Methodology, Resources. Validation, Writing review & editing. XJ: Conceptualization, Resources, Validation, Writing review & editing, Supervision. ZZ: Conceptualization, Methodology, Formal analysis, Writing review & editing, Supervision, Funding acquisition. All authors read and approved the final manuscript. All authors have participated sufficiently in the work and agreed to be accountable for all aspects of the work.

Ethics Approval and Consent to Participate

All experimental procedures were approved by the Institutional Animal Care and Use Committee of the Institute of Acupuncture and Moxibustion, China Academy of Chinese Medical Sciences (approval no. D2024-01-26-09) and conducted in accordance with the National Institutes of Health Guide for the Care and Use of Laboratory Animals.

Acknowledgment

We gratefully acknowledge the technical advice from Yani Li, Liaoyuxian Deng, and Junkang Chen.

Funding

This work was supported by National Natural Science Foundation of China [grant number 82204796], and the Fundamental Research Funds for the China Academy of Chinese Medical Sciences [grant number ZZ18-YQ-045].

Conflict of Interest

The authors declare no conflict of interest.

Declaration of AI and AI-Assisted Technologies in the Writing Process

During the preparation of this work the authors used Claude in order to check spell and grammar. After using this tool, the authors reviewed and edited the content as needed and takes full responsibility for the content of the publication.

Supplementary Material

Supplementary material associated with this article can be found, in the online version, at https://doi.org/10.31083/JIN46163.

References

[1] Chirila AM, Rankin G, Tseng SY, Emanuel AJ, Chavez-Martinez CL, Zhang D, *et al*. Mechanoreceptor signal convergence and transformation in the dorsal horn flexibly shape a di-

versity of outputs to the brain. Cell. 2022; 185: 4541–4559.e23. https://doi.org/10.1016/j.cell.2022.10.012.
[2] Koch SC, Acton D, Goulding M. Spinal Circuits for Touch, Pain, and Itch. Annual Review of Physiology. 2018; 80: 189–217. https://doi.org/10.1146/annurev-physiol-022516-034303.
[3] Abraira VE, Kuehn ED, Chirila AM, Springel MW, Toliver AA, Zimmerman AL, *et al*. The Cellular and Synaptic Architecture of the Mechanosensory Dorsal Horn. Cell. 2017; 168: 295–310.e19. https://doi.org/10.1016/j.cell.2016.12.010.
[4] Wercberger R, Basbaum AI. Spinal cord projection neurons: a superficial, and also deep, analysis. Current Opinion in Physiology. 2019; 11: 109–115. https://doi.org/10.1016/j.cophys.2019.10.002.
[5] Allard J. Physiological properties of the lamina I spinoparabrachial neurons in the mouse. The Journal of Physiology. 2019; 597: 2097–2113. https://doi.org/10.1113/JP277447.
[6] Fujiwara Y, Koga K, Nakamura NH, Maruo K, Tachibana T, Furue H. Optogenetic inhibition of spinal inhibitory neurons facilitates mechanical responses of spinal wide dynamic range neurons and causes mechanical hypersensitivity. Neuropharmacology. 2024; 242: 109763. https://doi.org/10.1016/j.neuropharm.2023.109763.
[7] Condés-Lara M, Martínez-Lorenzana G, Espinosa de Los Monteros-Zúñiga A, López-Córdoba G, Córdova-Quiroga A, Flores-Bojórquez SA, *et al*. Hypothalamic Paraventricular Stimulation Inhibits Nociceptive Wide Dynamic Range Trigeminocervical Complex Cells via Oxytocinergic Transmission. The Journal of Neuroscience: the Official Journal of the Society for Neuroscience. 2024; 44: e1501232024. https://doi.org/10.1523/JNEUROSCI.1501-23.2024.
[8] Morgan MM. Paradoxical inhibition of nociceptive neurons in the dorsal horn of the rat spinal cord during a nociceptive hindlimb reflex. Neuroscience. 1999; 88: 489–498. https://doi.org/10.1016/s0306-4522(98)00238-3.
[9] Sullivan SJ, Sdrulla AD. Excitatory and Inhibitory Neurons of the Spinal Cord Superficial Dorsal Horn Diverge in Their Somatosensory Responses and Plasticity *in Vivo*. The Journal of Neuroscience: the Official Journal of the Society for Neuroscience. 2022; 42: 1958–1973. https://doi.org/10.1523/JNEUROSCI.1860-21.2021.
[10] Rivera-Arconada I, Baccei ML, López-García JA, Bardoni R. An electrophysiologist's guide to dorsal horn excitability and pain. Frontiers in Cellular Neuroscience. 2025; 19: 1548252. https://doi.org/10.3389/fncel.2025.1548252.
[11] Greenspon CM, Battell EE, Devonshire IM, Donaldson LF, Chapman V, Hathway GJ. Lamina-specific population encoding of cutaneous signals in the spinal dorsal horn using multielectrode arrays. The Journal of Physiology. 2019; 597: 377–397. https://doi.org/10.1113/JP277036.
[12] Blanche TJ, Spacek MA, Hetke JF, Swindale NV. Polytrodes: high-density silicon electrode arrays for large-scale multiunit recording. Journal of Neurophysiology. 2005; 93: 2987–3000. https://doi.org/10.1152/jn.01023.2004.
[13] Parvathy SS, Masocha W. Gait analysis of C57BL/6 mice with complete Freund's adjuvant-induced arthritis using the CatWalk system. BMC Musculoskeletal Disorders. 2013; 14: 14. https://doi.org/10.1186/1471-2474-14-14.
[14] Dixon WJ. Efficient analysis of experimental observations. Annual Review of Pharmacology and Toxicology. 1980; 20: 441–462. https://doi.org/10.1146/annurev.pa.20.040180.002301.
[15] Chaplan SR, Bach FW, Pogrel JW, Chung JM, Yaksh TL. Quantitative assessment of tactile allodynia in the rat paw. Journal of Neuroscience Methods. 1994; 53: 55–63. https://doi.org/10.1016/0165-0270(94)90144-9.
[16] Menétrey D, Giesler GJ, Jr, Besson JM. An analysis of response properties of spinal cord dorsal horn neurones to nonnoxious and noxious stimuli in the spinal rat. Experimental Brain Research. 1977; 27: 15–33. https://doi.org/10.1007/BF00234822.
[17] Vrinten DH, Hamers FFT. 'CatWalk' automated quantitative gait analysis as a novel method to assess mechanical allodynia in the rat; a comparison with von Frey testing. Pain. 2003; 102: 203–209. https://doi.org/10.1016/s0304-3959(02)00382-2.
[18] Hunt SP, Pini A, Evan G. Induction of c-fos-like protein in spinal cord neurons following sensory stimulation. Nature. 1987; 328: 632–634. https://doi.org/10.1038/328632a0.
[19] Albisetti GW, Ganley RP, Pietrafesa F, Werynska K, Magalhaes de Sousa M, Sipione R, *et al*. Inhibitory Kcnip2 neurons of the spinal dorsal horn control behavioral sensitivity to environmental cold. Neuron. 2023; 111: 92–105.e5. https://doi.org/10.1016/j.neuron.2022.10.008.
[20] Allen Reference Atlas – Mouse Spinal Cord Atlas [brain atlas]. Available from https://atlas.brain-map.org/.(Accessed: 16 October 2025).
[21] Barrot M. Tests and models of nociception and pain in rodents. Neuroscience. 2012; 211: 39–50. https://doi.org/10.1016/j.neuroscience.2011.12.041.
[22] Feehan AK, Zadina JE. Morphine immunomodulation prolongs inflammatory and postoperative pain while the novel analgesic ZH853 accelerates recovery and protects against latent sensitization. Journal of Neuroinflammation. 2019; 16: 100. https://doi.org/10.1186/s12974-019-1480-x.
[23] Hu X, Du L, Liu S, Lan Z, Zang K, Feng J, *et al*. A TRPV4-dependent neuroimmune axis in the spinal cord promotes neuropathic pain. The Journal of Clinical Investigation. 2023; 133: e161507. https://doi.org/10.1172/JCI161507.
[24] Muramatsu Y, Sasho T, Saito M, Yamaguchi S, Akagi R, Mukoyama S, *et al*. Preventive effects of hyaluronan from deterioration of gait parameters in surgically induced mice osteoarthritic knee model. Osteoarthritis and Cartilage. 2014; 22: 831–835. https://doi.org/10.1016/j.joca.2014.03.016.
[25] D'Mello R, Dickenson AH. Spinal cord mechanisms of pain. British Journal of Anaesthesia. 2008; 101: 8–16. https://doi.org/10.1093/bja/aen088.
[26] Häring M, Zeisel A, Hochgerner H, Rinwa P, Jakobsson JET, Lönnerberg P, *et al*. Neuronal atlas of the dorsal horn defines its architecture and links sensory input to transcriptional cell types. Nature Neuroscience. 2018; 21: 869–880. https://doi.org/10.1038/s41593-018-0141-1.
[27] Targowska-Duda KM, Peters D, Marcus JL, Zribi G, Toll L, Ozawa A. Functional and anatomical analyses of active spinal circuits in a mouse model of chronic pain. Pain. 2024; 165: 685–697. https://doi.org/10.1097/j.pain.0000000000003068.
[28] Zhang MD, Kupari J, Su J, Magnusson KA, Hu Y, Calvo-Enrique L, *et al*. Neural ensembles that encode nocifensive mechanical and heat pain in mouse spinal cord. Nature Neuroscience. 2025; 28: 1012–1023. https://doi.org/10.1038/s41593-025-01921-6.
[29] Corbett BF, You JC, Zhang X, Pyfer MS, Tosi U, Iascone DM, *et al*. ΔFosB Regulates Gene Expression and Cognitive Dysfunction in a Mouse Model of Alzheimer's Disease. Cell Reports. 2017; 20: 344–355. https://doi.org/10.1016/j.celrep.2017.06.040.
[30] Stephens GS, Park J, Eagle A, You J, Silva-Pérez M, Fu CH, *et al*. Persistent ΔFosB expression limits recurrent seizure activity and provides neuroprotection in the dentate gyrus of APP mice. Progress in Neurobiology. 2024; 237: 102612. https://doi.org/10.1016/j.pneurobio.2024.102612.
[31] Zhang H, Zhang G, Xiao M, Cui S, Jin C, Yang J, *et al*. Two-polarized roles of transcription factor FOSB in lung cancer progression and prognosis: dependent on p53 status. Journal of Experimental & Clinical Cancer Research: CR. 2024; 43: 237. https://doi.org/10.1186/s13046-024-03161-1.

[32] Duque-Wilckens N, Maradiaga N, Szu-Ying Y, Joseph D, Srinavasan V, Thelen K, *et al*. Activity-dependent FosB gene expression negatively regulates mast cell functions. bioRxiv. 2024. https://doi.org/10.1101/2024.05.06.592755. (preprint)
[33] Shekhtmeyster P, Carey EM, Duarte D, Ngo A, Gao G, Nelson NA, *et al*. Multiplex translaminar imaging in the spinal cord of behaving mice. Nature Communications. 2023; 14: 1427. https://doi.org/10.1038/s41467-023-36959-2.
[34] Wang H, Chen W, Dong Z, Xing G, Cui W, Yao L, *et al*. A novel spinal neuron connection for heat sensation. Neuron. 2022; 110: 2315–2333.e6. https://doi.org/10.1016/j.neuron.2022.04.021.
[35] Tashima R, Koga K, Yoshikawa Y, Sekine M, Watanabe M, Tozaki-Saitoh H, *et al*. A subset of spinal dorsal horn interneurons crucial for gating touch-evoked pain-like behavior. Proceedings of the National Academy of Sciences of the United States of America. 2021; 118: e2021220118. https://doi.org/10.1073/pnas.2021220118.
[36] He Z, Zhang J, Xu J, Wang Y, Zheng X, Wang W. Differential Neuronal Activation of Nociceptive Pathways in Neuropathic Pain After Spinal Cord Injury. Cellular and Molecular Neurobiology. 2025; 45: 18. https://doi.org/10.1007/s10571-025-01532-6.
[37] Ma YC, Kang ZB, Shi YQ, Ji WY, Zhou WM, Nan W. The Complexity of Neuropathic Pain and Central Sensitization: Exploring Mechanisms and Therapeutic Prospects. Journal of Integrative Neuroscience. 2024; 23: 89. https://doi.org/10.31083/j.jin2305089.
[38] Ochoa JL, Yarnitsky D. Mechanical hyperalgesias in neuropathic pain patients: dynamic and static subtypes. Annals of Neurology. 1993; 33: 465–472. https://doi.org/10.1002/ana.410330509.
[39] Koltzenburg M, Lundberg LER, Torebjörk EH. Dynamic and static components of mechanical hyperalgesia in human hairy skin. Pain. 1992; 51: 207–219. https://doi.org/10.1016/0304-3959(92)90262-A.
[40] Field MJ, Bramwell S, Hughes J, Singh L. Detection of static and dynamic components of mechanical allodynia in rat models of neuropathic pain: are they signalled by distinct primary sensory neurones? Pain. 1999; 83: 303–311. https://doi.org/10.1016/s0304-3959(99)00111-6.
[41] Duan B, Cheng L, Bourane S, Britz O, Padilla C, Garcia-Campmany L, *et al*. Identification of spinal circuits transmitting and gating mechanical pain. Cell. 2014; 159: 1417–1432. https://doi.org/10.1016/j.cell.2014.11.003.
[42] Cheng L, Duan B, Huang T, Zhang Y, Chen Y, Britz O, *et al*. Identification of spinal circuits involved in touch-evoked dynamic mechanical pain. Nature Neuroscience. 2017; 20: 804–814. https://doi.org/10.1038/nn.4549.
[43] Tiwari V, Anderson M, Yang F, Tiwari V, Zheng Q, He SQ, *et al*. Peripherally Acting μ-Opioid Receptor Agonists Attenuate Ongoing Pain-associated Behavior and Spontaneous Neuronal Activity after Nerve Injury in Rats. Anesthesiology. 2018; 128: 1220–1236. https://doi.org/10.1097/ALN.0000000000002191.
[44] Cui X, Liu J, Uniyal A, Xu Q, Zhang C, Zhu G, *et al*. Enhancing spinal cord stimulation-induced pain inhibition by augmenting endogenous adenosine signalling after nerve injury in rats. British Journal of Anaesthesia. 2024; 132: 746–757. https://doi.org/10.1016/j.bja.2024.01.005.
[45] Turecek J, Lehnert BP, Ginty DD. The encoding of touch by somatotopically aligned dorsal column subdivisions. Nature. 2022; 612: 310–315. https://doi.org/10.1038/s41586-022-05470-x.
[46] Rankin G, Chirila AM, Emanuel AJ, Zhang Z, Woolf CJ, Drugowitsch J, *et al*. Nerve injury disrupts temporal processing in the spinal cord dorsal horn through alterations in PV^+ interneurons. Cell Reports. 2024; 43: 113718. https://doi.org/10.1016/j.celrep.2024.113718.
[47] Le Bars D. The whole body receptive field of dorsal horn multireceptive neurones. Brain Research. Brain Research Reviews. 2002; 40: 29–44. https://doi.org/10.1016/s0165-0173(02)00186-8.
[48] Craig ADB. Pain mechanisms: labeled lines versus convergence in central processing. Annual Review of Neuroscience. 2003; 26: 1–30. https://doi.org/10.1146/annurev.neuro.26.041002.131022.
[49] Medrano MC, Dhanasobhon D, Yalcin I, Schlichter R, Cordero-Erausquin M. Loss of inhibitory tone on spinal cord dorsal horn spontaneously and nonspontaneously active neurons in a mouse model of neuropathic pain. Pain. 2016; 157: 1432–1442. https://doi.org/10.1097/j.pain.0000000000000538.
[50] Daniele CA, MacDermott AB. Low-threshold primary afferent drive onto GABAergic interneurons in the superficial dorsal horn of the mouse. The Journal of Neuroscience: the Official Journal of the Society for Neuroscience. 2009; 29: 686–695. https://doi.org/10.1523/JNEUROSCI.5120-08.2009.
[51] Price TJ, Prescott SA. Inhibitory regulation of the pain gate and how its failure causes pathological pain. Pain. 2015; 156: 789–792. https://doi.org/10.1097/j.pain.0000000000000139.
[52] Warwick C, Salsovic J, Hachisuka J, Smith KM, Sheahan TD, Chen H, *et al*. Cell type-specific calcium imaging of central sensitization in mouse dorsal horn. Nature Communications. 2022; 13: 5199. https://doi.org/10.1038/s41467-022-32608-2.
[53] Zeilhofer HU, Zeilhofer UB. Spinal dis-inhibition in inflammatory pain. Neuroscience Letters. 2008; 437: 170–174. https://doi.org/10.1016/j.neulet.2008.03.056.
[54] Takazawa T, Choudhury P, Tong CK, Conway CM, Scherrer G, Flood PD, *et al*. Inhibition Mediated by Glycinergic and GABAergic Receptors on Excitatory Neurons in Mouse Superficial Dorsal Horn Is Location-Specific but Modified by Inflammation. The Journal of Neuroscience: the Official Journal of the Society for Neuroscience. 2017; 37: 2336–2348. https://doi.org/10.1523/JNEUROSCI.2354-16.2017.
[55] Boyle KA, Gradwell MA, Yasaka T, Dickie AC, Polgár E, Ganley RP, *et al*. Defining a Spinal Microcircuit that Gates Myelinated Afferent Input: Implications for Tactile Allodynia. Cell Reports. 2019; 28: 526–540.e6. https://doi.org/10.1016/j.celrep.2019.06.040.
[56] Stachowski NJ, Dougherty KJ. Spinal Inhibitory Interneurons: Gatekeepers of Sensorimotor Pathways. International Journal of Molecular Sciences. 2021; 22: 2667. https://doi.org/10.3390/ijms22052667.
[57] Kumeta Y, Murata K, Kitahata LM, Aoki M, Nishio Y, Collins JG. Fentanyl suppression of nociceptive neurons in the superficial dorsal horn of the cat. Anesthesiology. 1988; 69: 371–376. https://doi.org/10.1097/00000542-198809000-00014.
[58] Seagrove LC, Suzuki R, Dickenson AH. Electrophysiological characterisations of rat lamina I dorsal horn neurones and the involvement of excitatory amino acid receptors. Pain. 2004; 108: 76–87. https://doi.org/10.1016/j.pain.2003.12.004.
[59] Donovan-Rodriguez T, Dickenson AH, Urch CE. Gabapentin normalizes spinal neuronal responses that correlate with behavior in a rat model of cancer-induced bone pain. Anesthesiology. 2005; 102: 132–140. https://doi.org/10.1097/00000542-200501000-00022.
[60] Smith-Edwards KM, DeBerry JJ, Saloman JL, Davis BM, Woodbury CJ. Profound alteration in cutaneous primary afferent activity produced by inflammatory mediators. eLife. 2016; 5: e20527. https://doi.org/10.7554/eLife.20527.
[61] Xie RG, Chu WG, Liu DL, Wang X, Ma SB, Wang F, *et al*. Presynaptic NMDARs on spinal nociceptor terminals state-dependently modulate synaptic transmission and pain. Nature Communications. 2022; 13: 728. https://doi.org/10.1038/s41467-022-28429-y.

[62] Nakatsuka T, Park JS, Kumamoto E, Tamaki T, Yoshimura M. Plastic changes in sensory inputs to rat substantia gelatinosa neurons following peripheral inflammation. Pain. 1999; 82: 39–47. https://doi.org/10.1016/S0304-3959(99)00037-8.

[63] Zain M, Bonin RP. Alterations in evoked and spontaneous activity of dorsal horn wide dynamic range neurons in pathological pain: a systematic review and analysis. Pain. 2019; 160: 2199–2209. https://doi.org/10.1097/j.pain.0000000000001632.

[64] Urch CE, Dickenson AH. In vivo single unit extracellular recordings from spinal cord neurones of rats. Brain Research. Brain Research Protocols. 2003; 12: 26–34. https://doi.org/10.1016/s1385-299x(03)00068-0.

[65] Yang F, Zhang C, Xu Q, Tiwari V, He SQ, Wang Y, *et al*. Electrical stimulation of dorsal root entry zone attenuates wide-dynamic-range neuronal activity in rats. Neuromodulation: Journal of the International Neuromodulation Society. 2015; 18: 33–40; discussion 40. https://doi.org/10.1111/ner.12249.

[66] Yang F, Xu Q, Cheong YK, Shechter R, Sdrulla A, He SQ, *et al*. Comparison of intensity-dependent inhibition of spinal wide-dynamic range neurons by dorsal column and peripheral nerve stimulation in a rat model of neuropathic pain. European Journal of Pain (London, England). 2014; 18: 978–988. https://doi.org/10.1002/j.1532-2149.2013.00443.x.

[67] McGaraughty S, Chu KL, Xu J. Characterization and pharmacological modulation of noci-responsive deep dorsal horn neurons across diverse rat models of pathological pain. Journal of Neurophysiology. 2018; 120: 1893–1905. https://doi.org/10.1152/jn.00325.2018.

[68] Coghill RC, Mayer DJ, Price DD. Wide dynamic range but not nociceptive-specific neurons encode multidimensional features of prolonged repetitive heat pain. Journal of Neurophysiology. 1993; 69: 703–716. https://doi.org/10.1152/jn.1993.69.3.703.

[69] Fan J, Li X, Wang P, Yang F, Zhao B, Yang J, *et al*. A Hyperflexible Electrode Array for Long-Term Recording and Decoding of Intraspinal Neuronal Activity. Advanced Science (Weinheim, Baden-Wurttemberg, Germany). 2023; 10: e2303377. https://doi.org/10.1002/advs.202303377.